arXiv:1605.05324v1 [astro-ph.HE] 17 May 2016

MINUTE-TIMESCALE > 100 MeV γ-RAY VARIABILITY DURING THE GIANT OUTBURST OF QUASAR 3C 279 OBSERVED BY *Fermi*-LAT IN 2015 JUNE

M. Ackermann[1], R. Anantua[2], K. Asano[3], L. Baldini[4,2], G. Barbiellini[5,6], D. Bastieri[7,8], J. Becerra Gonzalez[9,10], R. Bellazzini[11], E. Bissaldi[12], R. D. Blandford[2], E. D. Bloom[2], R. Bonino[13,14], E. Bottacini[2], P. Bruel[15], R. Buehler[1], G. A. Caliandro[2,16], R. A. Cameron[2], M. Caragiulo[17,12], P. A. Caraveo[18], E. Cavazzuti[19], C. Cecchi[20,21], C. C. Cheung[22], J. Chiang[2], G. Chiaro[8], S. Ciprini[19,20], J. Cohen-Tanugi[23], F. Costanza[12], S. Cutini[19,20], F. D'Ammando[24,25], F. de Palma[12,26], R. Desiante[27,13], S. W. Digel[2], N. Di Lalla[11], M. Di Mauro[2], L. Di Venere[17,12], P. S. Drell[2], C. Favuzzi[17,12], S. J. Fegan[15], E. C. Ferrara[9], Y. Fukazawa[28], S. Funk[29], P. Fusco[17,12], F. Gargano[12], D. Gasparrini[19,20], N. Giglietto[17,12], F. Giordano[17,12], M. Giroletti[24], I. A. Grenier[30], L. Guillemot[31,32], S. Guiriec[9,33], M. Hayashida[3,*], E. Hays[9], D. Horan[15], G. Jóhannesson[35], S. Kensei[28], D. Kocevski[9], M. Kuss[11], S. La Mura[8], S. Larsson[36,37], L. Latronico[13], J. Li[38], F. Longo[5,6], F. Loparco[17,12], B. Lott[39], M. N. Lovellette[22], P. Lubrano[20], G. M. Madejski[2,*], J. D. Magill[10], S. Maldera[13], A. Manfreda[11], M. Mayer[1], M. N. Mazziotta[12], P. F. Michelson[2], N. Mirabal[9,33], T. Mizuno[40], M. E. Monzani[2], A. Morselli[41], I. V. Moskalenko[2], K. Nalewajko[42,*], M. Negro[13,14], E. Nuss[23], T. Ohsugi[40], E. Orlando[2], D. Paneque[43,2], J. S. Perkins[9], F. Piron[23], G. Pivato[11], T. A. Porter[2], G. Principe[29], R. Rando[7,8], M. Razzano[11,44], S. Razzaque[45], A. Reimer[46,2], J. D. Scargle[47], C. Sgrò[11], M. Sikora[42], D. Simone[12], E. J. Siskind[48], F. Spada[11], P. Spinelli[17,12], L. Stawarz[49], J. B. Thayer[2], D. J. Thompson[9], D. F. Torres[38,50], E. Troja[9,10], Y. Uchiyama[51], Y. Yuan[2], S. Zimmer[52]

Accepted for Publication in ApJL

ABSTRACT

On 2015 June 16, *Fermi*-LAT observed a giant outburst from the flat spectrum radio quasar 3C 279 with a peak > 100 MeV flux of ∼ 3.6×10^{-5} photons cm^{-2} s^{-1} averaged over orbital period intervals. It is the historically highest γ-ray flux observed from the source including past EGRET observations, with the γ-ray isotropic luminosity reaching ∼ 10^{49} erg s^{-1}. During the outburst, the *Fermi* spacecraft, which has an orbital period of 95.4 min, was operated in a special pointing mode to optimize the exposure for 3C 279. For the first time, significant flux variability at sub-orbital timescales was found in blazar observations by *Fermi*-LAT. The source flux variability was resolved down to 2-min binned timescales, with flux doubling times less than 5 min. The observed minute-scale variability suggests a very compact emission region at hundreds of Schwarzschild radii from the central engine in conical jet models. A minimum bulk jet Lorentz factor (Γ) of 35 is necessary to avoid both internal γ-ray absorption and super-Eddington jet power. In the standard external-radiation-Comptonization scenario, Γ should be at least 50 to avoid overproducing the synchrotron-self-Compton component. However, this predicts extremely low magnetization (∼ 5×10^{-4}). Equipartition requires Γ as high as 120, unless the emitting region is a small fraction of the dissipation region. Alternatively, we consider γ rays originating as synchrotron radiation of $\gamma_e \sim 1.6 \times 10^6$ electrons, in magnetic field $B \sim$ 1.3 kG, accelerated by strong electric fields $E \sim B$ in the process of magnetoluminescence. At such short distance scales, one cannot immediately exclude production of γ rays in hadronic processes.

Keywords: galaxies: active — galaxies: jets — gamma rays: galaxies — quasars: individual (3C 279) — radiation mechanisms: non-thermal

* Corresponding authors: M. Hayashida, mahaya@icrr.u-tokyo.ac.jp; G. M. Madejski, madejski@slac.stanford.edu; K. Nalewajko, knalew@camk.edu.pl

[1] Deutsches Elektronen Synchrotron DESY, D-15738 Zeuthen, Germany

[2] W. W. Hansen Experimental Physics Laboratory, Kavli Institute for Particle Astrophysics and Cosmology, Department of Physics and SLAC National Accelerator Laboratory, Stanford University, Stanford, CA 94305, USA

[3] Institute for Cosmic-Ray Research, University of Tokyo, 5-1-5 Kashiwanoha, Kashiwa, Chiba, 277-8582, Japan

[4] Università di Pisa and Istituto Nazionale di Fisica Nucleare, Sezione di Pisa I-56127 Pisa, Italy

[5] Istituto Nazionale di Fisica Nucleare, Sezione di Trieste, I-34127 Trieste, Italy

[6] Dipartimento di Fisica, Università di Trieste, I-34127 Trieste, Italy

[7] Istituto Nazionale di Fisica Nucleare, Sezione di Padova, I-35131 Padova, Italy

[8] Dipartimento di Fisica e Astronomia "G. Galilei", Università di Padova, I-35131 Padova, Italy

[9] NASA Goddard Space Flight Center, Greenbelt, MD 20771, USA

[10] Department of Physics and Department of Astronomy, University of Maryland, College Park, MD 20742, USA

[11] Istituto Nazionale di Fisica Nucleare, Sezione di Pisa, I-56127 Pisa, Italy

[12] Istituto Nazionale di Fisica Nucleare, Sezione di Bari, I-70126 Bari, Italy

[13] Istituto Nazionale di Fisica Nucleare, Sezione di Torino, I-10125 Torino, Italy

[14] Dipartimento di Fisica Generale "Amadeo Avogadro" , Università degli Studi di Torino, I-10125 Torino, Italy

[15] Laboratoire Leprince-Ringuet, École polytechnique, CNRS/IN2P3, F-91128 Palaiseau, France

[16] Consorzio Interuniversitario per la Fisica Spaziale (CIFS), I-10133 Torino, Italy

[17] Dipartimento di Fisica "M. Merlin" dell'Università e del Politecnico di Bari, I-70126 Bari, Italy

[18] INAF-Istituto di Astrofisica Spaziale e Fisica Cosmica, I-20133 Milano, Italy

[19] Agenzia Spaziale Italiana (ASI) Science Data Center, I-00133 Roma, Italy

[20] Istituto Nazionale di Fisica Nucleare, Sezione di Perugia, I-06123 Perugia, Italy

[21] Dipartimento di Fisica, Università degli Studi di Perugia, I-06123 Perugia, Italy

1. INTRODUCTION

Amongst all high-luminosity blazars — which are active galaxies dominated by Doppler-boosted emission from relativistic jets pointing toward our line of sight — 3C 279 is one of the most extensively studied objects. This flat spectrum radio quasar (FSRQ: $z = 0.536$) has been detected in essentially all accessible spectral bands; in particular, strong and variable γ-ray emission was detected by *Compton*/EGRET (Hartman et al. 1992; Kniffen et al. 1993), and it was the first FSRQ detected above 100 GeV (Albert et al. 2008). The γ-ray emission dominates the apparent luminosity of the source, and the nature of γ-ray variability and its relationship to that measured in other bands provide the strongest constraints on the total energetics as well as the emission processes operating in the jets of luminous blazars (e.g.,

[22] Space Science Division, Naval Research Laboratory, Washington, DC 20375-5352, USA
[23] Laboratoire Univers et Particules de Montpellier, Université Montpellier, CNRS/IN2P3, F-34095 Montpellier, France
[24] INAF Istituto di Radioastronomia, I-40129 Bologna, Italy
[25] Dipartimento di Astronomia, Università di Bologna, I-40127 Bologna, Italy
[26] Università Telematica Pegaso, Piazza Trieste e Trento, 48, I-80132 Napoli, Italy
[27] Università di Udine, I-33100 Udine, Italy
[28] Department of Physical Sciences, Hiroshima University, Higashi-Hiroshima, Hiroshima 739-8526, Japan
[29] Erlangen Centre for Astroparticle Physics, D-91058 Erlangen, Germany
[30] Laboratoire AIM, CEA-IRFU/CNRS/Université Paris Diderot, Service d'Astrophysique, CEA Saclay, F-91191 Gif sur Yvette, France
[31] Laboratoire de Physique et Chimie de l'Environnement et de l'Espace – Université d'Orléans / CNRS, F-45071 Orléans Cedex 02, France
[32] Station de radioastronomie de Nançay, Observatoire de Paris, CNRS/INSU, F-18330 Nançay, France
[33] NASA Postdoctoral Program Fellow, USA
[35] Science Institute, University of Iceland, IS-107 Reykjavik, Iceland
[36] Department of Physics, KTH Royal Institute of Technology, AlbaNova, SE-106 91 Stockholm, Sweden
[37] The Oskar Klein Centre for Cosmoparticle Physics, AlbaNova, SE-106 91 Stockholm, Sweden
[38] Institute of Space Sciences (IEEC-CSIC), Campus UAB, E-08193 Barcelona, Spain
[39] Centre d'Études Nucléaires de Bordeaux Gradignan, IN2P3/CNRS, Université Bordeaux 1, BP120, F-33175 Gradignan Cedex, France
[40] Hiroshima Astrophysical Science Center, Hiroshima University, Higashi-Hiroshima, Hiroshima 739-8526, Japan
[41] Istituto Nazionale di Fisica Nucleare, Sezione di Roma "Tor Vergata", I-00133 Roma, Italy
[42] Nicolaus Copernicus Astronomical Center, 00-716 Warsaw, Poland
[43] Max-Planck-Institut für Physik, D-80805 München, Germany
[44] Funded by contract FIRB-2012-RBFR12PM1F from the Italian Ministry of Education, University and Research (MIUR)
[45] Department of Physics, University of Johannesburg, PO Box 524, Auckland Park 2006, South Africa
[46] Institut für Astro- und Teilchenphysik and Institut für Theoretische Physik, Leopold-Franzens-Universität Innsbruck, A-6020 Innsbruck, Austria
[47] Space Sciences Division, NASA Ames Research Center, Moffett Field, CA 94035-1000, USA
[48] NYCB Real-Time Computing Inc., Lattingtown, NY 11560-1025, USA
[49] Astronomical Observatory, Jagiellonian University, 30-244 Kraków, Poland
[50] Institució Catalana de Recerca i Estudis Avançats (ICREA), Barcelona, Spain
[51] Department of Physics, 3-34-1 Nishi-Ikebukuro, Toshima-ku, Tokyo 171-8501, Japan
[52] University of Geneva, Département de physique nucléacuteaire et corpusculaire (DPNC), 24 quai Ernest-Ansermet, CH-1211 Genève 4, Switzerland

Maraschi et al. 1992; Sikora et al. 1994).

Owing to the all-sky monitoring capability of the *Fermi* Large Area Telescope (LAT: Atwood et al. 2009), we have a continuous γ-ray flux history of 3C 279 for more than 7 years. 3C 279 underwent several outbursts in the past, having flared with a peak γ-ray flux ($E > 100$ MeV) $\sim 10^{-5}$ photons cm^{-2} s^{-1}, in 2013 December and 2014 April, with fluxes about three times greater than the peak during the first 2 years of *Fermi*-LAT observations (Hayashida et al. 2012, 2015). During the flaring epoch in 2013 December, the γ-ray spectrum hardened ($\Gamma_\gamma \simeq 1.7$ in dN/d$E \propto E^{-\Gamma_\gamma}$) and rapid hour-scale flux variability was observed. The γ-ray flux strongly dominated the flux in any other band, indicating a very high "Compton dominance" (the ratio of the total inverse-Compton luminosity over the total synchrotron luminosity) of a factor of 100. This in turn suggests extremely low jet magnetization, with a level of 10^{-4}. Those results motivated, e.g., the stochastic acceleration model, which could reproduce the hour-scale variability and the hard spectrum of the flare event (Asano & Hayashida 2015).

In 2015 June, 3C 279 became very active again with fluxes exceeding the 2013/2014 level (Cutini 2015; Paliya 2015), and prompting a Target of Opportunity (ToO) repointing of *Fermi*, resulting in a ~ 2.5 times greater exposure. The measured γ-ray flux in daily bins reached $\sim 2.4 \times 10^{-5}$ photons cm^{-2} s^{-1} on 2015 June 16, allowing an unprecedented investigation of variability on timescales even shorter than one *Fermi* orbit. In this Letter, we report and offer an interpretation of the minute-scale variability observed by *Fermi*-LAT for the first time in *any* blazar.

2. *Fermi*-LAT GAMMA-RAY OBSERVATIONS

We analyzed the LAT data following the standard procedure[53], using the LAT analysis software `ScienceTools v10r01p01` with the `P8R2_SOURCE_V6` instrument response functions. Events with energies 0.1–300 GeV were extracted within a 15° acceptance cone Region of Interest (ROI) centered at 3C 279 (RA = 195°.047, Dec=−5°.789, J2000). Gamma-ray spectra were derived by an unbinned maximum likelihood fit with `gtlike`. The background model included sources from the third LAT catalog (3FGL: Acero et al. 2015) inside the ROI and which showed TS> 25[54] based on an analysis of 1-month of LAT data, for 2015 June. Their spectral parameters were fixed by the fitting results from the 1-month data analysis. Additionally, the model included the isotropic and Galactic diffuse emission components[55](Acero et al. 2016), with fixed normalizations during the fitting. Note that the contribution of background components to the 3C 279 flux determinations in short-term binned light curves during the outburst is negligible.

2.1. *Light curve*

Figure 1 shows light curves of 3C 279 measured by *Fermi*-LAT between 2015 June 14 12:00:00 and June 18 00:00:00 UTC, including the most intense outburst observed on June 16. ToO observations were conducted from 2015 June 15 17:31:00 through 2015 June 23 16:19:00, during which LAT switched from its normal survey mode to a pointing mode

[53] http://fermi.gsfc.nasa.gov/ssc/data/analysis/
[54] "TS" stands for the test statistic from the likelihood ratio test (see Mattox et al. 1996).
[55] iso_P8R2_SOURCE_V6_v06.txt and gll_iem_v06.fits

targeting 3C 279. For data taken during the normal observing mode, the data were binned at a twice the orbital period so that individual bins can have more uniform exposure times. Beginning with the ToO observation, the data were binned orbit by orbit. The γ-ray fluxes and photon indices were derived using a simple power-law model. The hardness ratio in the 5th panel of Figure 1 was defined as the ratio between the hard-band (> 1 GeV) and the soft-band ($0.1-1$ GeV) fluxes; $F_{>1\,\mathrm{GeV}}/F_{0.1-1\,\mathrm{GeV}}$. Here we define the outburst phase to be between 2015 June 15 22:17:12 and June 16 15:46:36 (MJD 57188.92861 and 57189.65736) as indicated in Figure 1: it comprises 11 one-orbit bins designated Orbit 'A' to 'K' respectively.

The greatest flux above 100 MeV was recorded during Orbit C, centered at 2015 June 16 02:15:42 (MJD 57189.09424), reaching $(3.6 \pm 0.2) \times 10^{-5}$ photons cm^{-2} s^{-1}. It exceeds the largest 3C 279 flares previously detected by *Fermi*-LAT on 2013 December 20, 2014 April 4 (Hayashida et al. 2015; Paliya et al. 2015), and those detected by EGRET in 1996 (Wehrle et al. 1998) ($\sim 1.2 \times 10^{-5}$ photons cm^{-2} s^{-1}), making it the historical largest γ-ray (> 100 MeV) flare of 3C 279. It is the second-greatest flux among blazars observed by *Fermi*-LAT after the 3C 454.3 outburst in 2010 November (Abdo et al. 2011a). During Orbit C we found $\Gamma_\gamma = 2.01 \pm 0.05$, which was not as hard as $\Gamma_\gamma \sim 1.7$ observed on 2013 December 20. The hardest spectrum during this outburst was $\Gamma_\gamma = 1.91 \pm 0.07$ in Orbit B.

The highest-energy photon, 56 GeV, was detected[56] at 2015 June 16 14:58:12 UTC, almost at the end of the outburst phase (Figure 1, bottom), corresponding to ~ 15.1 hours since the outburst began, and ~ 12.7 hours later than the center of the highest-flux time bin. Interestingly, in the 2010 November flare of 3C 454.3, the highest-energy photon (31 GeV) also arrived during the decay part of the main flare (Abdo et al. 2011a).

2.2. *Sub-orbital scale variability*

The very high γ-ray flux state and the ToO observations provided a sufficiently large number of photons in each bin to resolve light curves with shorter timescales than the *Fermi* orbital period. Figure 2-(a) shows light curves above 100 MeV for integration times of 5 min (red) and 3 min (green) for Orbits B–J, where the orbit-averaged flux exceeded 2×10^{-5} photons cm^{-2} s^{-1}. The spacecraft location and attitude data with 1-s resolution were used for analysis of those short-timescale light curves. To investigate flux variability at sub-orbital periods, we fitted a constant value to each orbit for both time bins, and calculated a probability (p-value) from χ^2 in each orbit. While many orbits resulted in p-values consistent with constant fluxes, we found significant indications of variability on a sub-orbital timescale for Orbit C: (p, χ^2/dof)=(0.0015, 19.62/5) and (0.00047, 29.8/9) for 5- and 3-min bins respectively, and Orbit D: (p, χ^2/dof)=(0.067, 11.79/6) and (0.068, 18.65/11) for 5- and 3-min bins, respectively (see details in Table 1).

Enlarged views of light curves above 100 MeV for Orbits C and D are in Figure 2-(b); those show integration times of 3 min and 2 min. In those time bins, the flux reached $\sim 5 \times 10^{-5}$ photons cm^{-2} s^{-1} at the highest, and showed most rapid variations. In the 3-min binned light curve, the flux dou-

---

[56] probability of association with 3C 279 estimated by `gtsrcprob` is $> 99.99\%$

bled even from the 3rd to the 4th bins, and decreased by almost a half from the 6th to the 7th bins. Although defining the characteristic timescale of the variability is difficult, the flux doubling time is conservatively less than 10 min, and plausibly ~ 5 min or shorter.

2.3. *Power Density Spectrum*

The available LAT data allow us to study the Power Density Spectrum (PDS) on different timescales. Results for three different frequency ranges are shown in Figure 3. Two lower-frequency (< 0.1 day^{-1}) PDSs were calculated, each from a 3-day binned light curve covering one half of the 7-year LAT data (MJD 54683–55950 and 55950–57254, respectively). The PDS for intermediate frequencies is based on a light curve for the active period in 2015 June (MJD 57181–57197) binned on the orbital period of *Fermi*. White noise subtraction was based on the estimated measurement errors in the light curves and these were also logarithmically binned before plotting in Figure 3. The PDS's for high frequencies were derived from the 3-min binned sub-orbital light curves of Orbits B–J. One PDS was calculated for each orbit, and then these were averaged. White noise defined from the flat PDS level above 110 days^{-1} has been subtracted. The normalization of the PDS means that if the rms/flux is constant during variations in source flux, the PDS level will not change. The intermediate frequency PDS connects well with the low-frequency PDS for the second 3.5 years, which includes the active period in 2015 June. The PDS for the second 3.5-year interval shows a higher relative variability and a flatter spectrum (slope: -0.61 ± 0.06) compared to the first interval (slope: -1.24 ± 0.15) as well as a break around 0.1 day^{-1}.

2.4. *Gamma-ray Spectra*

Gamma-ray spectra measured by *Fermi*-LAT, extracted for each orbit during the outburst, were fitted to simple power-law (PL) and log-parabola (LP: $dN/dE \propto (E/E_0)^{-\alpha - \beta \log(E/E_0)}$ with $E_0 = 300$ MeV) models (see Table 1). The peak energy (E_{peak}) of the spectral energy distribution (SED) was derived from a fit with the LP model. Generally, the LP model is more favored than the PL model to describe the spectral shape. The fitting results suggest that E_{peak} ranges between ~ 300 MeV and ~ 1 GeV during the outburst. At the beginning and end of the outburst, the spectra appear relatively hard with SED peaks at ~ 1 GeV. The SED peaks were located at significantly higher energies than for the usual states of 3C 279, when the peak is located below the *Fermi*-LAT band (< 100 MeV), but lower than E_{peak} observed in the 2013 December 20 flare ($\gtrsim 3$ GeV).

Figure 4 shows the γ-ray SED as measured by *Fermi*-LAT for each orbit. In these plots, Orbits F and G, and Orbits H and I, were combined because they showed similar spectral fitting results and fluxes. The spectra in the "*pre-outburst*" and "*post-flare*" periods as defined in Figure 1 were also extracted for comparison. The spectral peaks are apparently located within the LAT energy band during the outburst. The peak SED flux reaches nearly $\sim 10^{-8}$ erg cm^{-2} s^{-1}, corresponding to an apparent luminosity of 10^{49} erg s^{-1}.

3. DISCUSSION

For the first time, *Fermi*-LAT detected variability of > 100 MeV γ-ray flux from a blazar on timescales of $t_{\mathrm{var,obs}} \sim 5$ min or shorter. These timescales are comparable to the shortest variability timescales detected above

100 GeV in a handful of blazars and a radio galaxy by ground-based Cherenkov telescopes (PKS 2155−304, Aharonian et al. 2007; Mrk 501, Albert et al. 2007; IC 310, Aleksić et al. 2014). Moreover, this is only the second case when such timescales are reported for an FSRQ blazar, after PKS 1222+216 (Aleksić et al. 2011), while *Fermi*-LAT had only ever detected variability as short as hour timescales in some FSRQs (e.g., Abdo et al. 2011a; Saito et al. 2013; Hayashida et al. 2015). This observational result imposes very stringent constraints on the parameters of the γ-ray emitting region.

Emitting region size — The observed variability timescale constrains the characteristic size of the emitting region radius $R_\gamma < \mathcal{D}ct_{\rm var,obs}/(1+z) \simeq 10^{-4}(\mathcal{D}/50)$ pc, where $\mathcal{D}$ is the Doppler factor. With such extremely short variability timescale, we may consider a significantly larger dissipation region (a region from which energy is transferred/supplied to the emitting regions) of $R_{\rm diss} = R_\gamma/f_\gamma$, where f_γ is a scale factor. Normally, $f_\gamma = 1$; however, values of order $f_\gamma \sim 0.01 - 0.1$ are motivated, e.g., by studies of relativistic magnetic reconnection (Cerutti et al. 2012; Nalewajko et al. 2012). The corresponding characteristic distance scale along the jet for a conical geometry is $r_{\rm diss} \simeq R_{\rm diss}/\theta \simeq 0.005(\Gamma/50)^2(\mathcal{D}/\Gamma)(\Gamma\theta)^{-1}f_\gamma^{-1}$ pc, where Γ is the Lorentz factor, and θ is the opening angle. This corresponds to ~ 100 Schwarzschild radii ($R_{\rm S}$) for a black hole mass of $M_{\rm BH} \sim 5 \times 10^8 \,{\rm M}_\odot$ (as adopted in Hayashida et al. 2015), and is generally well within the broad-line region (BLR) with $r_{\rm BLR} \sim 0.1$ pc (Tavecchio et al. 2010). While it is typical to assume that $\mathcal{D} \simeq \Gamma$ and $\Gamma\theta \simeq 1$, larger distance scales can be obtained for $\Gamma\theta < 1$ (see also Saito et al. 2015).

Jet energetics — The total jet power required to produce the γ-ray emission of apparent luminosity $L_\gamma \sim 10^{49}$ erg s^{-1} is $L_{\rm j} \simeq L_\gamma/(\eta_{\rm j}\Gamma^2) \sim 4 \times 10^{46}(\Gamma/50)^{-2}(\eta_{\rm j}/0.1)^{-1}$ erg s^{-1}, where $\eta_{\rm j}$ is the radiative jet efficiency, typically ~ 0.1 (Nemmen et al. 2012). The jet power will exceed the Eddington luminosity of $L_{\rm Edd} \sim 8 \times 10^{46}$ erg s^{-1} for $\Gamma < 35(\eta_{\rm j}/0.1)^{-1/2}$.

Internal absorption — The optical depth for internal γ-ray absorption is given by $\tau_{\gamma\gamma,\rm int} \simeq (1+z)^2\sigma_{\rm T}L_{\rm soft}E_{\rm max,obs}/(72\pi m_e^2c^6\mathcal{D}^6t_{\rm var})$ (Dondi & Ghisellini 1995; Begelman et al. 2008). Excluding a single $\simeq 56$ GeV photon, several photons were detected during the outburst with energies in the range 10–15 GeV, and hence we adopt a maximum photon energy of $E_{\rm max,obs} = 15$ GeV. Based on the *Swift*-XRT observation performed during Orbit D (obsID 35019180), which resulted in a high source flux of $(5.5 \pm 0.2) \times 10^{-11}$ erg cm^{-2} s^{-1} with a hard photon index of $\Gamma_{\rm X} = 1.17 \pm 0.06$ (for the 0.5–5 keV band) and $L_{\rm X} \sim 10^{47}$ erg s^{-1}, a soft radiation (~ 17 keV) luminosity of $L_{\rm soft} \sim 3 \times 10^{47}$ erg s^{-1} has been adopted. The minimum Doppler factor corresponding to $\tau_{\gamma\gamma,\rm int} = 1$ is $\mathcal{D}_{\rm min,int} \simeq 25$.

External absorption — External radiation fields can absorb the γ-ray photons observed at $E_{\rm max,obs}$ when $E_{\rm ext} > 2(m_ec^2)^2/[(1-\mu)(1+z)E_{\rm max,obs}] \simeq 23/(1-\mu)$ eV in the source frame ($\mu = \cos\theta_{\rm scat}$, $\theta_{\rm scat}$:scattering angle). At short distance scales $R_{\rm diss} \ll r_{\rm BLR}$, additional absorption may arise from the UV or soft X-ray radiation produced by the accretion disk or its corona (Dermer et al. 1992), radiation reprocessed by the surrounding medium (Blandford & Levinson 1995), or from

high-ionization He II lines (Poutanen & Stern 2010). However, the observed photon statistics are insufficient to derive quantitative results for the absorption.

ERC scenario — In the standard leptonic model of FS-RQs, γ rays are produced by the External Radiation Comptonization (ERC) mechanism (e.g., Sikora et al. 2009). This requires that leptons are accelerated to Lorentz factors of $\gamma_e \simeq [(1+z)E_{\rm obs}/(\mathcal{D}\Gamma E_{\rm ext})]^{1/2} \simeq 250(\Gamma/50)^{-1}(E_{\rm ext}/10 \text{ eV})^{-1/2}$. The radiative cooling timescale satisfies $t'_{\rm cool}(\gamma_e) \simeq 3m_ec/(4\sigma_{\rm T}\gamma_e u'_{\rm ext}) \lesssim t'_{\rm var}$ for the minimum energy density of external radiation fields $u'_{\rm ext,min} \simeq 3m_ec/(4\sigma_{\rm T}t_{\rm var,obs})[(1+z)E_{\rm ext}/E_{\rm cool,obs}]^{1/2} \sim 40 \text{ erg cm}^{-3}$. This minimum energy density can be provided by broad emission lines ($u'_{\rm BLR} \simeq 0.37\Gamma^2\xi_{\rm BLR}$ erg cm^{-3}; Hayashida et al. 2012) for $\Gamma > 33$, assuming a covering factor of $\xi_{\rm BLR} \sim 0.1$. The same leptons would also produce a synchrotron component peaking in the mid-IR band at luminosity $L_{\rm syn} \sim L_\gamma/q$, where $q \sim 100$ is the Compton dominance, and a synchrotron self-Compton (SSC) component peaking in the hard X-ray band at luminosity $L_{\rm SSC} \sim L_\gamma^2/(4\pi cq\mathcal{D}^4R_\gamma^2u'_{\rm ext})$ (Nalewajko et al. 2014). $L_{\rm SSC}$ would exceed the X-ray luminosity observed by *Swift*-XRT for jet Lorentz factors $\Gamma < 46$. The magnetic jet power can be estimated as $L_{\rm B} = \pi R_{\rm diss}^2\Gamma^2u'_{\rm BLR}c/q \simeq 2 \times 10^{43}(\Gamma/50)^6f_\gamma^{-2}$ erg s$^{-1} \sim 0.0005(\Gamma/50)^8f_\gamma^{-2}(\eta_{\rm j}/0.1)L_{\rm j}$. Hence, the jet Lorentz factor $\Gamma = 50$, while satisfying the Eddington, opacity, cooling, and SSC constraints — and already much higher than the value inferred from radio observations, $\Gamma_{\rm var} \simeq 21$ (Hovatta et al. 2009) — corresponds to severe matter domination. However, since $L_{\rm B}/L_{\rm j} \propto \Gamma^8$, equipartition defined as $L_{\rm B} = L_{\rm j}/2$ (Dermer et al. 2014) can be obtained for $\Gamma_{\rm eqp} \simeq 120f_\gamma^{1/4}$.

Synchrotron scenario — Alternatively, we consider a more exotic scenario, in which γ rays are produced as synchrotron radiation by energetic electrons in a strong magnetic field — in addition to the standard synchrotron component produced under typical conditions — motivated by the γ-ray flares of the Crab Nebula (Abdo et al. 2011b), and also investigated in the context of the 100 GeV emission from FSRQ PKS 1222+216 (Nalewajko et al. 2012). This scenario requires leptons accelerated to Lorentz factors $\gamma_e \simeq [(1+z)E_{\rm obs}/(20{\rm neV} \times \mathcal{D}B')]^{1/2} \simeq 1.6 \times 10^6(E_{\rm obs}/1 \text{ GeV})^{1/2}(\Gamma/25)f_\gamma^{-1/2}$, where the magnetic field strength can be estimated from the equipartition magnetic jet power as $B' \simeq (1+z)f_\gamma(8L_{\rm B}/c)^{1/2}/(\Gamma^2ct_{\rm var,obs}) \simeq 1.3 \text{ kG} \times (\Gamma/25)^{-3}f_\gamma$. With such energetic leptons, the inverse-Compton scattering proceeds in the Klein-Nishina regime, and neither SSC or ERC components are important. A high bulk Lorentz factor $\Gamma \simeq 25$ is still required for avoiding internal absorption of γ rays and it is helpful for pushing the observed synchrotron photon energy limit to comfortable values $E_{\rm syn,max} \simeq 4 \text{ GeV} \times (\Gamma/25)(E'_\parallel/B'_\perp)$ (e.g., Cerutti et al. 2012). Particle acceleration in magnetic reconnection sites with $E'_\parallel > B'_\perp$ (Kirk 2004; Uzdensky et al. 2011) is not necessary. The synchrotron cooling timescale is ~ 3 ms in the comoving frame, placing this scenario in the fast cooling regime. This will result in a low-energy electron tail $N(\gamma_e) \propto \gamma_e^{-2}$, and a corresponding spectral tail $EF(E) \propto E^{0.5}$.

Hadronic scenarios — On the very small distance scales, the radiative efficiency of the proton-initiated cascade mech-

anism (Mannheim & Biermann 1992) is enhanced due to very dense target radiation fields, and that of the proton-synchrotron mechanism (Aharonian 2000) is enhanced due to very strong magnetic fields ($B' \gtrsim$ kG). A careful analysis of these mechanisms, including the non-linear feedback effects (Petropoulou & Mastichiadis 2012), requires a dedicated study.

Dissipation mechanism — The observed variability timescale and luminosity require extremely efficient bulk jet acceleration within $\sim 100\,R_S$. In the synchrotron scenario, they also require extremely efficient particle acceleration, going beyond the established picture of the blazar sequence (Ghisellini et al. 1998). Magnetic reconnection was invoked as a dissipation focusing mechanism effectively increasing the scale of the dissipation region by $f_\gamma^{-1} \sim 10$–100 (Cerutti et al. 2012). Relativistic reconnection can also produce relativistic outflows dubbed 'minijets', which can provide additional local Lorentz boost (Giannios et al. 2009). In general, magnetic dissipation can lead to rapid conversion of magnetic energy to radiation by the process called *magnetoluminescence* (Blandford et al. 2015).

4. SUMMARY

In this Letter, we reported the first minute-timescale γ-ray flux variability observed by *Fermi*-LAT in an FSRQ blazar, 3C 279. In the standard ERC scenario with conical jet geometry, the minute-scale variability requires a high Γ (> 50) and extremely low magnetization even at the jet base ($\sim 100\,R_S$) or $\Gamma \sim 120$ under equipartition. The high Γ and/or low magnetization at the jet base pose challenges to standard models of electromagnetically driven jets. We also discuss an alternative, synchrotron origin for the GeV γ-ray outburst, which would work in a magnetically dominated jet, but requires higher electron energies and still implies $\Gamma \sim 25$ at the jet base.

REFERENCES

Abdo, A. A., Ackermann, M., Ajello, M., et al. 2011a, ApJL, 733, L26
Abdo, A. A., Ackermann, M., Ajello, M., et al. 2011b, Science, 331, 739
Acero, F., Ackermann, M., Ajello, M., et al. 2015, ApJS, 218, 23
Acero, F., Ackermann, M., Ajello, M., et al. 2016, ApJS, 223, 26
Aharonian, F. A. 2000, New A, 5, 377
Aharonian, F., Akhperjanian, A. G., Bazer-Bachi, A. R., et al. 2007, ApJL, 664, L71
Albert, J., Aliu, E., Anderhub, H., et al. 2007, ApJ, 669, 862
Albert, J., Aliu, E., Anderhub, H., et al. 2008, Science, 320, 1752
Aleksić, J., Antonelli, L. A., Antoranz, P., et al. 2011, ApJL, 730, L8
Aleksić, J., Ansoldi, S., Antonelli, L. A., et al. 2014, Science, 346, 1080
Asano, K., & Hayashida, M. 2015, ApJL, 808, L18
Atwood, W. B., et al. 2009, ApJ, 697, 1071
Begelman, M. C., Fabian, A. C., Rees, M. J., 2008, MNRAS, 384, L19
Blandford, R. D., & Levinson, A. 1995, ApJ, 441, 79
Blandford, R. D., Yuan, Y., & Zrake, J. 2015, AAS, 225, 214.07
Cerutti, B., Werner, G. R., Uzdensky, D. A., & Begelman, M. C. 2012, ApJ, 754, L33
Cutini, S. 2015, The Astronomer's Telegram, 7633,
Dermer, C. D., Schlickeiser, R., & Mastichiadis, A., 1992, A&A, 256, L27
Dermer, C. D., Cerruti, M., Lott, B., Boisson, C., & Zech, A. 2014, ApJ, 782, 82
Dondi, L., & Ghisellini, G. 1995, MNRAS, 273, 583
Ghisellini, G., Celotti, A., Fossati, G., Maraschi, L., & Comastri, A. 1998, MNRAS, 301, 451
Giannios, D., Uzdensky, D. A., & Begelman, M. C., 2009, MNRAS, 395, L29
Hartman, R. C., Bertsch, D. L., Fichtel, C. E., et al. 1992, ApJL, 385, L1
Hayashida, M., Madejski, G. M., Nalewajko, K., et al. 2012, ApJ, 754, 114
Hayashida, M., Nalewajko, K., Madejski, G. M., et al. 2015, ApJ, 807, 79
Hovatta, T., Valtaoja, E., Tornikoski, M., Lähteenmäki, A. 2009, A&A, 494, 527
Kirk, J. G., 2004, PhRvL, 92, 181101
Kniffen, D. A., Bertsch, D. L., Fichtel, C. E., et al. 1993, ApJ, 411, 133
Mannheim, K., & Biermann, P. L. 1992, A&A, 253, L21
Maraschi, L., Ghisellini, G., & Celotti, A. 1992, ApJL, 397, L5
Mattox, J. R., Bertsch, D. L., Chiang, J., et al. 1996, ApJ, 461, 396
Nalewajko, K., Begelman, M. C., Cerutti, B., Uzdensky, D. A., & Sikora, M. 2012, MNRAS, 425, 2519
Nalewajko, K., Begelman, M. C., & Sikora, M. 2014, ApJ, 789, 161
Nemmen, R. S., Georganopoulos, M., Guiriec, S., et al. 2012, Science, 338, 1445
Paliya, V. S., Sahayanathan, S., & Stalin, C. S. 2015, ApJ, 803, 15
Paliya, V. S. 2015, ApJL, 808, L48
Petropoulou, M., & Mastichiadis, A. 2012, MNRAS, 426, 462
Poutanen, J., & Stern, B., 2010, ApJ, 717, L118
Saito, S., Stawarz, Ł., Tanaka, Y. T., et al. 2013, ApJL, 766, L11
Saito, S., Stawarz, Ł., Tanaka, Y. T., et al. 2015, ApJ, 809, 171
Sikora, M., Begelman, M. C., & Rees, M. J. 1994, ApJ, 421, 153
Sikora, M., Stawarz, Ł., Moderski, R., Nalewajko, K., & Madejski, G. M. 2009, ApJ, 704, 38
Tavecchio, F., Ghisellini, G., Bonnoli, G., & Ghirlanda, G. 2010, MNRAS, 405, L94
Uzdensky, D. A., Cerutti, B., & Begelman, M. C. 2011, ApJ, 737, L40
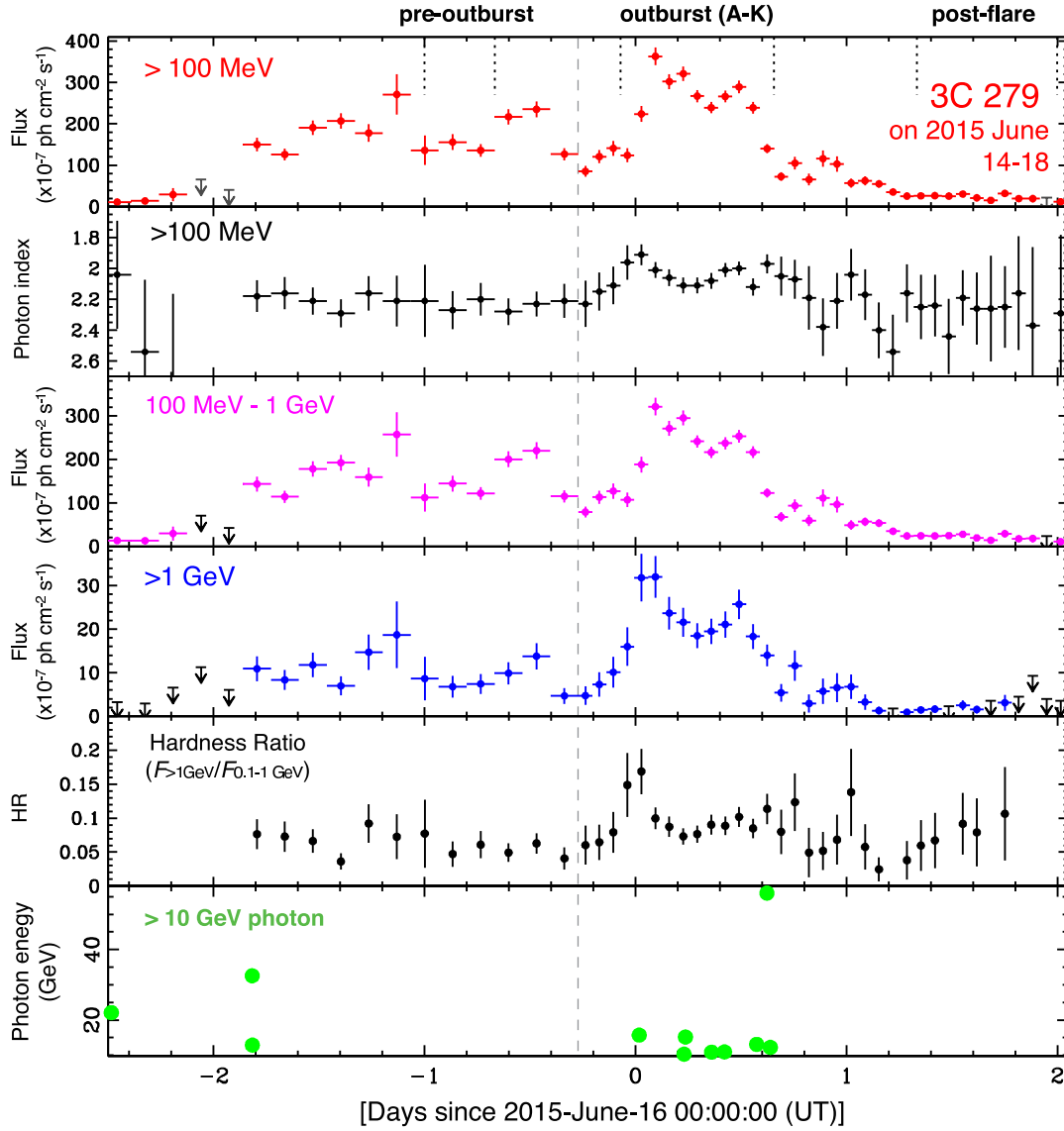Wehrle, A. E., Pian, E., Urry, C. M., et al. 1998, ApJ, 497, 178

Figure 1. Light curves of 3C 279 in the γ-ray band as observed by *Fermi*-LAT. The vertical dashed line indicates when the *Fermi*-LAT observation mode was switched from the normal survey mode to the pointing mode of the ToO observations. The data were binned on a two-orbit timescale (190.8 min) during the normal survey mode and on a one-orbit timescale (95.4 min) during the ToO observations. The panels from the top to the bottom show: (1) integrated flux above 100 MeV, (2) photon index above 100 MeV, (3) integrated flux between 0.1 and 1 GeV ($F_{0.1-1\,\mathrm{GeV}}$), (4) integrated flux above 1 GeV ($F_{>1\,\mathrm{GeV}}$), (5) hardness ratio ($F_{>1\,\mathrm{GeV}}/F_{0.1-1\,\mathrm{GeV}}$), (6) arrival time distribution of photons with reconstructed energies above 10 GeV. For bins with TS< 6, 95% confidence level upper limits are plotted.
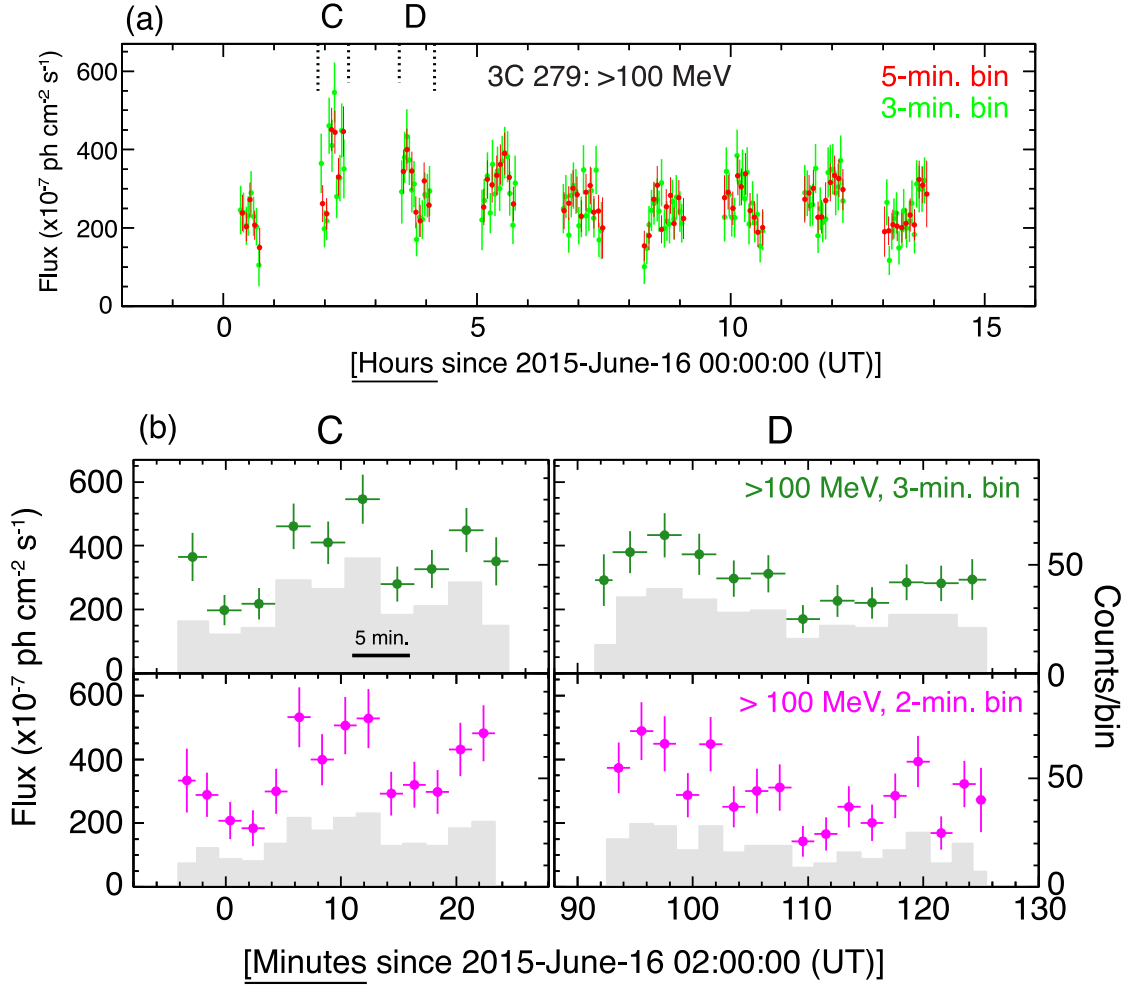
Figure 2. Light curves of 3C 279 above 100 MeV with minute-timescale intervals. (a): Intervals of 5 min (red) and 3 min (green) during the outburst phase from Orbits B–J. (b): Enlarged view during Orbits C and D. Each range is indicated with dotted vertical lines in (a). The points denote the fluxes (left axis), and the gray shaded histograms represent numbers of events (right axis) detected within 8° radius centered at 3C 279 for each bin. Contamination from both diffuse components were estimated as ∼ 1 photon for each 3-min bin.
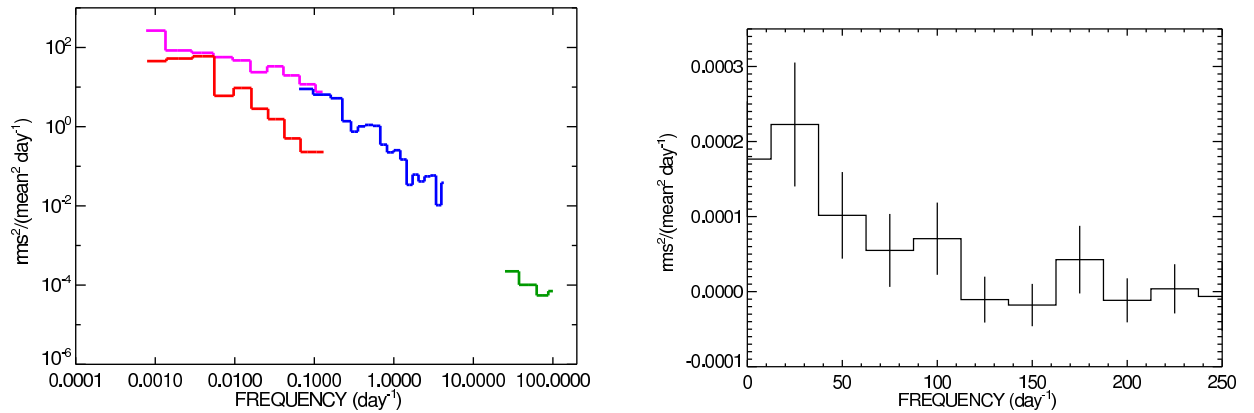

Figure 3. Power Density Spectrum (PDS) of the γ-ray flux of 3C 279. (left) PDS derived from three different time-binned light curves: 3 days (red and magenta), orbital period (blue) and 3 min (green). The PDS's marked in red and magenta were derived using the first and second halves of the first 7-year *Fermi*-LAT observation, respectively. The second half of the interval contains the giant outburst phase in 2015 June. (right) Enlarged view of the high-frequency part of the PDS, based on 3-min binned light curves, plotted using a linear scale and including also the highest frequencies. The white noise level has been subtracted.
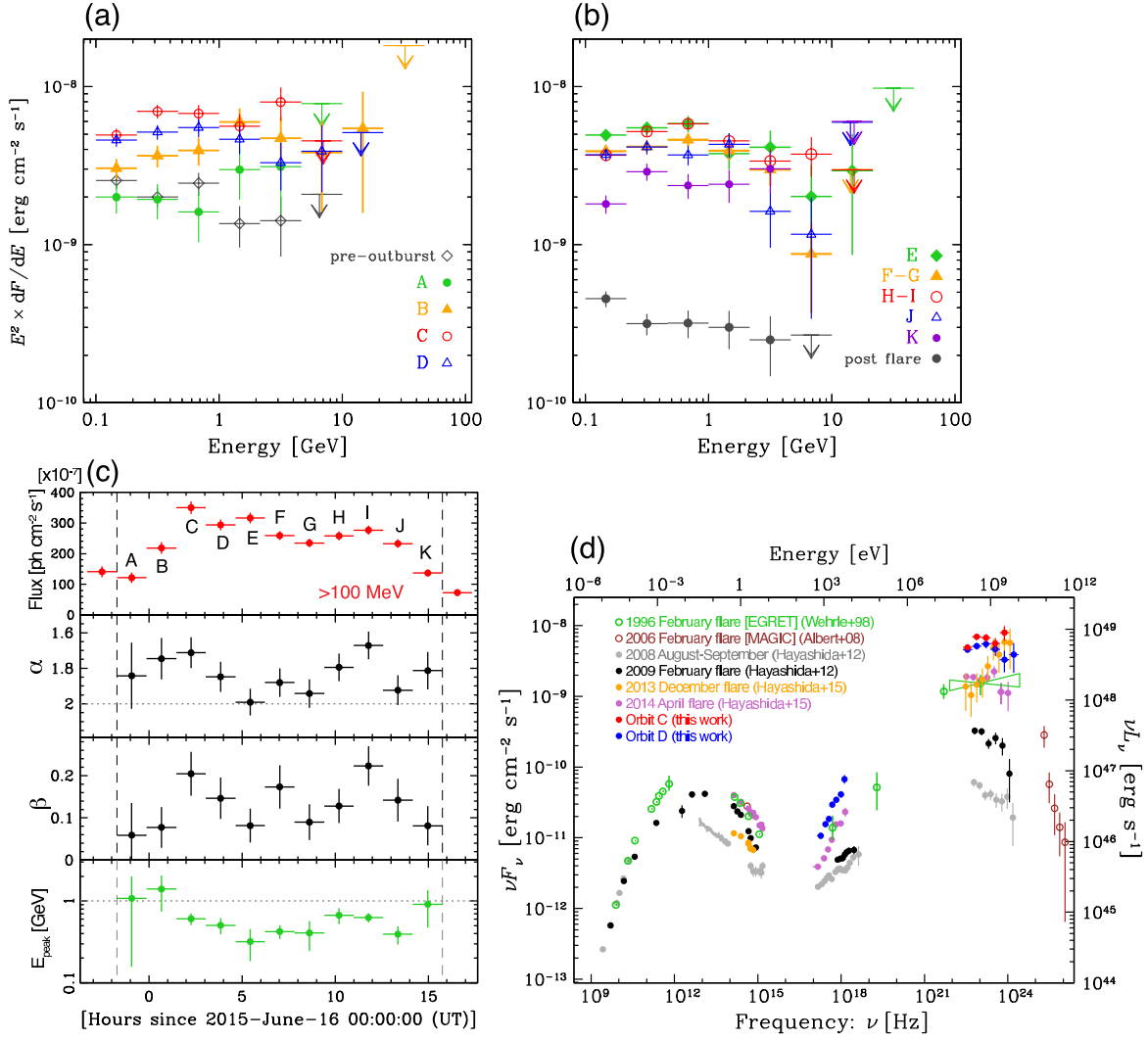
Figure 4. (a,b): Gamma-ray SEDs of 3C 279 for each orbit during the outburst phase as well as "*pre-outburst*" and "*post flare*" as indicated in Figure 1. The down arrows represent 95% confidence level upper limits. (c): Best fit parameters of the spectra based on the log-parabola model for each orbit (see Table 1 for numbers). (d) Broad-band SED of Orbit C and D, and some historical multi-band observations with EGRET, MAGIC and *Fermi*-LAT.

Table 1
Flux and spectral fitting results of 3C 279 above 100 MeV for each orbit (A–K) during the outburst phase.

Orbit number	Flux[a] (10^{-7})	Γ_γ (PL[b])	α (LP[b])	β (LP[b])	E_{peak} (GeV)	TS	$-2\Delta L$[c]	p-value[d] (5 min. bin)	p-value[d] (3 min. bin)	E_{max} (GeV)
A	121 ± 17	1.96 ± 0.11	1.84 ± 0.19	0.06 ± 0.08	1.1 ± 0.9	502	0.7	$\cdots$	$\cdots$	8.8
B	218 ± 19	1.91 ± 0.07	1.75 ± 0.12	0.08 ± 0.05	1.40 ± 0.66	1346	3.2	0.434	0.453	16.9
C	350 ± 21	2.01 ± 0.05	1.71 ± 0.09	0.20 ± 0.05	0.61 ± 0.10	3037	21.9	0.00148	0.000474	9.3
D	294 ± 18	2.06 ± 0.05	1.85 ± 0.09	0.15 ± 0.05	0.50 ± 0.11	2661	11.8	0.0668	0.0677	6.7
E	316 ± 17	2.11 ± 0.05	1.99 ± 0.08	0.08 ± 0.04	0.32 ± 0.14	3400	5.0	0.504	0.429	15.2
F	259 ± 14	2.11 ± 0.05	1.88 ± 0.08	0.17 ± 0.04	0.42 ± 0.08	3036	15.6	0.902	0.419	9.2
G	235 ± 14	2.08 ± 0.05	1.94 ± 0.08	0.09 ± 0.04	0.41 ± 0.16	2720	5.6	0.166	0.308	10.9
H	258 ± 14	2.01 ± 0.05	1.79 ± 0.08	0.13 ± 0.04	0.67 ± 0.15	3309	13.4	0.228	0.140	10.9
I	277 ± 15	2.00 ± 0.04	1.67 ± 0.08	0.22 ± 0.05	0.63 ± 0.08	3699	32.8	0.708	0.435	7.7
J	233 ± 14	2.12 ± 0.05	1.92 ± 0.08	0.14 ± 0.05	0.39 ± 0.10	2630	10.3	0.404	0.177	13.1
K	137 ± 11	1.97 ± 0.06	1.81 ± 0.11	0.08 ± 0.05	0.91 ± 0.44	1540	3.8	$\cdots$	$\cdots$	56.0

[a] Orbit-averaged flux above 100 MeV in photons cm^{-2} s^{-1}.
[b] PL: power-law model, LP: log-parabola model.
[c] ΔL represents the difference of the logarithm of the total likelihood of the fits between PL and LP models.
[d] p-value based on χ^2 fits with a constant flux to each orbit for 5-min. and 3-min. binned light curves.